USCAP

www.nature.com/labinvest

ARTICLE

Collagen XVII deficiency alters epidermal patterning

Yunan Wang[1], Hiroyuki Kitahata[2], Hideyuki Kosumi[1], Mika Watanabe[1,3], Yu Fujimura[1], Shota Takashima[1], Shin-Ichi Osada[4], Tomonori Hirose[5], Wataru Nishie[1], Masaharu Nagayama[6], Hiroshi Shimizu[1] and Ken Natsuga[1]✉

Vertebrates exhibit patterned epidermis, exemplified by scales/interscales in mice tails and grooves/ridges on the human skin surface (microtopography). Although the role of spatiotemporal regulation of stem cells (SCs) has been implicated in this process, the mechanism underlying the development of such epidermal patterns is poorly understood. Here, we show that collagen XVII (COL17), a niche for epidermal SCs, helps stabilize epidermal patterns. Gene knockout and rescue experiments revealed that COL17 maintains the width of the murine tail scale epidermis independently of epidermal cell polarity. Skin regeneration after wounding was associated with slender scale epidermis, which was alleviated by overexpression of human COL17. COL17-negative skin in human junctional epidermolysis bullosa showed a distinct epidermal pattern from COL17-positive skin that resulted from revertant mosaicism. These results demonstrate that COL17 contributes to defining mouse tail scale shapes and human skin microtopography. Our study sheds light on the role of the SC niche in tissue pattern formation.

Laboratory Investigation (2022) 102:581–588; https://doi.org/10.1038/s41374-022-00738-2

INTRODUCTION

The skin is the body's outermost organ and is composed of the multilayered epithelium, the epidermis, and the underlying dermis. The epidermis serves as a physical barrier to pathogens and prevents water leakage from the body[1]. The epidermis is maintained by a fine-tuned balance between the proliferation and differentiation of epidermal stem cells (SCs), which reside in the epidermal basal layer[2]. Epidermal SCs need niche proteins such as integrins and collagen XVII (COL17) for their proper function[3,4]. Functional loss of these proteins leads to transient hyperproliferation of the developing epidermis due to disturbed SC maintenance[5–7].

Vertebrates have distinct skin patterns. In some, the patterns are visible through melanin distribution in the skin (e.g., zebra and tiger stripes); in others, the allocation of skin components forms patterns (e.g., human microtopography, hair follicles (HFs), and fish scales). Murine tail skin serves as a robust model for examining epidermal pattern formation[8]. The tail epidermis consists of scale (parakeratotic) and interscale (orthokeratotic) areas, which are arranged alternately. These scale and interscale areas are distinguished by the expression of keratin 31 (K31) and keratin 10 (K10), respectively[9]. Label-retaining and lineage-tracing experiments have revealed that K10+ interscale epidermis is slow-cycling, whereas K31+ scale areas are fast-cycling. Two distinct SC populations (Dlx1+ and Slc1a3+) give rise to interscale and scale epidermis, respectively[10], although it is unclear how these cell populations are arranged into scale/interscale patterns.

The expression of epidermal SC niche proteins, including integrins and COL17, shows alternate patterns in the human epidermis, where their expression is enriched in the epidermis facing the dermal protrusion but not in the epidermal rete ridges[11–13]. Conversely, the scale/interscale patterns are absent in β1 integrin-null tail epidermis[14]. These previous studies suggest the involvement of SC niche proteins in epidermal pattern formation. However, whether these SC niche proteins indeed regulate the epidermal patterns and the mechanisms underlying such regulation are unknown.

Here, we demonstrate that COL17, an SC niche protein[7,15–17], helps in the formation of proper epidermal patterns in mice and humans. Interestingly, disturbed epidermal patterning through COL17 deletion is independent of aberrant epidermal cell polarity, but could involve wound-related skin changes.

MATERIAL AND METHODS

Animals

C57BL/6 (wild-type, WT) mice were purchased from Clea (Tokyo, Japan). *Col17a1*−/−, K14-hCOL17 (h: human, a courtesy gift from Prof. Kim B Yancey), hCOL17+; *Col17a1*−/−, K5-Cre;*aPKCλ*$^{\Delta E5/\Delta E5}$ (aPKCλ eKO), and *Prkcz*−/− (aPKCζ KO) were generated as previously described[18–21]. aPKCλ$^{\Delta E5/\Delta E5}$ and *Prkcz*+/− mice were used as aPKCλ eKO and aPKCζ KO controls, respectively. aPKCλ eKO and aPKCλ$^{\Delta E5/\Delta E5}$ littermates were generated by mating aPKCλ eKO and aPKCλ$^{\Delta E5/\Delta E5}$ mice. aPKCζ KO and *Prkcz*+/− littermates were generated by mating aPKCζ KO and *Prkcz*+/− mice. Littermate *Col17a1*+/− or *Col17a1*+/+ mice were used as *Col17a1*−/− or hCOL17+;*Col17a1*−/− control. *Col17a1*−/−, *Col17a1*+/−, and *Col17a1*+/+ littermates were generated by mating *Col17a1*+/− female and male mice. hCOL17+; *Col17a1*−/−, *Col17a1*+/−, and *Col17a1*+/+ littermates were generated by mating hCOL17+;*Col17a1*+/− and *Col17a1*+/− mice. K14-hCOL17 and WT littermates were generated by mating K14-hCOL17 and WT mice. Female mice were used for the wound-healing experiments on WT mice. Otherwise,

[1]Department of Dermatology, Faculty of Medicine and Graduate School of Medicine, Hokkaido University, Sapporo, Japan. [2]Department of Physics, Graduate School of Science, Chiba University, Chiba, Japan. [3]Department of Life Sciences and Systems Biology, Molecular Biotechnology Centre, University of Turin, Turin, Italy. [4]Department of Dermatology, Nippon Medical School, Tokyo, Japan. [5]Department of Molecular Biology, Yokohama City University Graduate School of Medicine, Yokohama, Japan. [6]Research Institute for Electronic Science, Hokkaido University, Sapporo, Japan. ✉email: natsuga@med.hokudai.ac.jp

Received: 8 July 2021 Revised: 14 January 2022 Accepted: 16 January 2022
Published online: 10 February 2022

sex-matched mice were used in each experiment. The institutional review board of the Hokkaido University Graduate School of Medicine approved all animal studies described below.

Cell culture

hTERT-immortalized human primary keratinocytes (KerCT; ATCC, Manassas, VA, USA), and spontaneously transformed murine keratinocytes (PAM212)[22] were cultured in serum-free keratinocyte growth medium (KGM; Lonza). The cells were transfected with 10 μM of human *COL17A1* siRNA, murine *Col17a1* siRNA or the control (Mock) (Silencer Select siRNAs, Thermo Fisher Scientific, Waltham, MA, USA) using Lipofectamine 2000 (Thermo Fisher Scientific) and Opti-MEM (Thermo Fisher Scientific). The cells were analyzed at 48 or 72 h after the knockdown procedure.

Antibodies

The following antibodies were used: polyclonal anti-K31 (Progen, hHa1), polyclonal anti-K10 (BioLegend, Poly19054), polyclonal anti-K6 (BioLegend, Poly19057), monoclonal anti-cytoplasmic COL17 (Abcam, Cambridge, MA, USA, ab186415/EPR14758).

Quantitative RT-PCR (qRT-PCR)

RNA was isolated from the tail epidermis or cultured cells using the RNeasy Mini kit (QIAGEN, Hilden, Germany), and cDNA was synthesized using the SuperScript III First-Strand Synthesis System (Thermo Fisher Scientific, Waltham, MA, USA). qRT-PCR was carried out using the designated primers and fast SYBR Green (Thermo Fisher Scientific) in a STEP-One Plus sequence detection system (Applied Biosystems, Waltham, MA, USA).

The following primers were used for the analysis: Forward primer and reverse primer are: murine *Krt6a*, CACGTTAAGAAGCAGTGTGCC and GCTCTGAGCACGGGATTCT; murine *Krt6b*, AGGAGTGCAGGTTGAATGGTG and AAAAAGAGAAGCGAGAGGACACA; murine *Krt16*, TCCCAGCTCAGCATGAAAG and GAGCTGTGGATATTCTCGCCA; murine *Krt17*, AGACAGAGAACCGCTACTGC and CGGGTGGTCACAGGTTCTTTT; murine *Col17a1*, GATGGCACTGAAGTCACCGA and TATCCATTGCTGGTGCTCCC; murine *Cyc1*, ATCGTTCGAGCTAGGCATGG and GCCGGGAAAGTAAGGGTTGA; human *KRT17*, CAGAGAACCGCTACTGCGTG and GTCACCGGTTCTTTCTTGTACTG; human *KRT16*, GCTCAGCATGAAAGCATCCC and GACCTCGCGGGAAGAATAGG; human *KRT6A*, AGTGCAGGCTGAATGGCGAA and TGGGACCGAGAGCTAGCAGA; human *KRT6B*, TTCATCGACAAGGTGCGGT and CAGCTCCGAGTCCAGACGAC; human *COL17A1*, TCAACCAGAGGACGGAGTCA and TCGACTCCCCTTGAGCAAAC; human *RNA18SN1* (18S), GGCGCCCCCTCGATGCTCTTAG and GCTCGGGCCTGCTTTGAACACTCT.

Immunofluorescence staining

Paraffin sections were deparaffinized and boiled in citrate or EDTA buffer for 20 min in a microwave oven. Frozen sections or cultured cells were fixed in 4% paraformaldehyde (PFA) for 10 min at room temperature (RT), or cold acetone or used without fixation. After washing with PBS, sections were treated with blocking buffer (0.5% fish skin gelatine, 5% goat serum, 4% BSA in PBS) for 1 h. The samples were incubated with primary antibodies at 4 °C overnight and were subsequently incubated with secondary antibodies conjugated with Alexa fluor 488, Alexa fluor 647, or FITC at RT for 1 h. Nuclei were stained with 4′,6-diamidino-2-phenylindole (DAPI). Images were obtained using confocal microscopy (FV1000, Olympus, Tokyo, Japan; LSM-710, Zeiss, Germany) or fluorescence microscopy (BZ-9000, Keyence, Osaka, Japan).

Whole-mount staining

Tail skin was incubated in 5 mM EDTA/PBS on a shaker at 37 °C for 4 h to separate the epidermis from the dermis. Epidermal sheets were fixed in 4% PFA for 1 h at RT. After blocking, epidermal sheets were incubated with primary antibodies overnight at RT, and then washed in 0.2% Tween/PBS. Samples were subsequently incubated with secondary antibodies. After washing, epidermal sheets were mounted on glass slides in Mowiol solution. The images of whole-mount stained samples were obtained using FV1000 confocal laser scanning microscope (Olympus, Tokyo, Japan) or BZ-9000 fluorescence microscope (Keyence, Osaka, Japan). The size and shape of the scales near the midline of the tail epidermis were analyzed using ImageJ (NIH, Bethesda, MD, USA). When the scales of the littermates were compared, the area, length, and width of the scales were normalized to the whole tail equivalents to exclude the effects of the organismal size of each mouse.

Wound-healing experiments

The surface of the tail skin (epidermis and papillary dermis, approximately 5 × 4 mm in size) was removed using a scalpel from 1-month-old (1MO) WT mice or K14-hCOL17 mice to produce superficial skin wounds (Supplementary Fig. 5A). The wounded skin was collected and analyzed when the healing process was complete (typically 4–6 weeks after wounding) and at a later time point (3 months after wounding).

Junctional epidermolysis bullosa (JEB) skin analysis

Photographs of the skin of a JEB patient[23] who was compound heterozygous for c.1179del (p.Ala394Leufs*9) and c.4159C>T (p.Gln1387*) in *COL17A1* (NM_000494.4) were taken by TG-5 (Olympus). Three revertant mosaicism spots and three adjacent diseased skin areas from the upper arm were further analyzed as described below. Although the fingerprints have been absent in other JEB patients with *COL17A1* p.Arg1303Gln mutations[24–26], the patient in our study maintained his fingerprints. This discrepancy is probably due to the difference of the *COL17A* mutations. The institutional review board of the Hokkaido University Graduate School of Medicine approved all human studies described above (ID: 13-043). The study was conducted according to the principles of the Declaration of Helsinki. The participant provided written informed consent.

Quantification of the skin microtopography

We selected several regions like the one surrounded by the red circle in the left panels of Supplementary Fig. 6A, B for Diseased skin and Reverted skin. We converted the image inside each circle to a grayscale image and calculated the two-dimensional autocorrelation function[27] (right panels in Supplementary Fig. 6A, B). Using the two-dimensional autocorrelation function, the characteristic direction of the epidermal pattern was detected by determining the direction in which the autocorrelation in the range of a distance less than 1 mm is the largest. The one-dimensional autocorrelation function was calculated (Supplementary Fig. 6C, D) in the direction perpendicular to the characteristic direction, represented by the red lines in the right panels in Supplementary Fig. 6A, B. The peak height (Δ) of the one-dimensional autocorrelation function in the range of distance less than 1 mm was adopted to quantify the regularity of the pattern. In the case where no peak was detected, the peak height was set to zero. The above-mentioned image analyses were performed with ImageJ NIH (Bethesda, MD, USA; https://imagej.nih.gov/ij/) by preparing a plug-in.

Statistical analysis

Statistical analysis was performed using GraphPad Prism (GraphPad Software, La Jolla, CA, USA). p values were determined using Welch's t test, Student's t test, or Mann–Whitney test. p values are indicated as *$0.01 < p < 0.05$, **$0.001 < p < 0.01$, ***$0.0001 < p < 0.001$, ****$p < 0.0001$. The values are shown as violin plots. Violin plots show median (dashed line) and quartiles (dotted line).

RESULTS

COL17 deficiency alters scale shape in the tail skin

We first characterized the scale/interscale patterning of *Col17a1*−/−[19] tail epidermis. We selected the time point of 1MO, when the scales became mature[8] (Supplementary Fig. 1). Immunofluorescence of the tail sections showed K10+ interscale and K31+ scale alternate patterns in both *Col17a1*−/− and controls (Fig. 1A; Supplementary Fig. 2A). We then examined the scale shape by whole skin imaging. We defined the length and width of a scale as the diameter of the anterior–posterior (AP) and lateral-medial (LM) axes, respectively (Fig. 1B). Since the length and width of whole tail samples varied among the mice (Supplementary Table 1), we normalized the scale length/width by dividing them by each mouse tail length/width to exclude the effects of organismal size in the analysis. Whole-mount imaging showed that the scale size was smaller and the shape was more slender (shorter on the LM axis) in the *Col17a1*−/− tail epidermis than in the littermate controls (Fig. 1C–F, Supplementary Fig. 2B). The shorter scale width in *Col17a1*−/− explains the smaller size of *Col17a1*−/− scales because their length was comparable to that of the controls (Fig. 1G, H). Although the basal cell number of maximum diameter

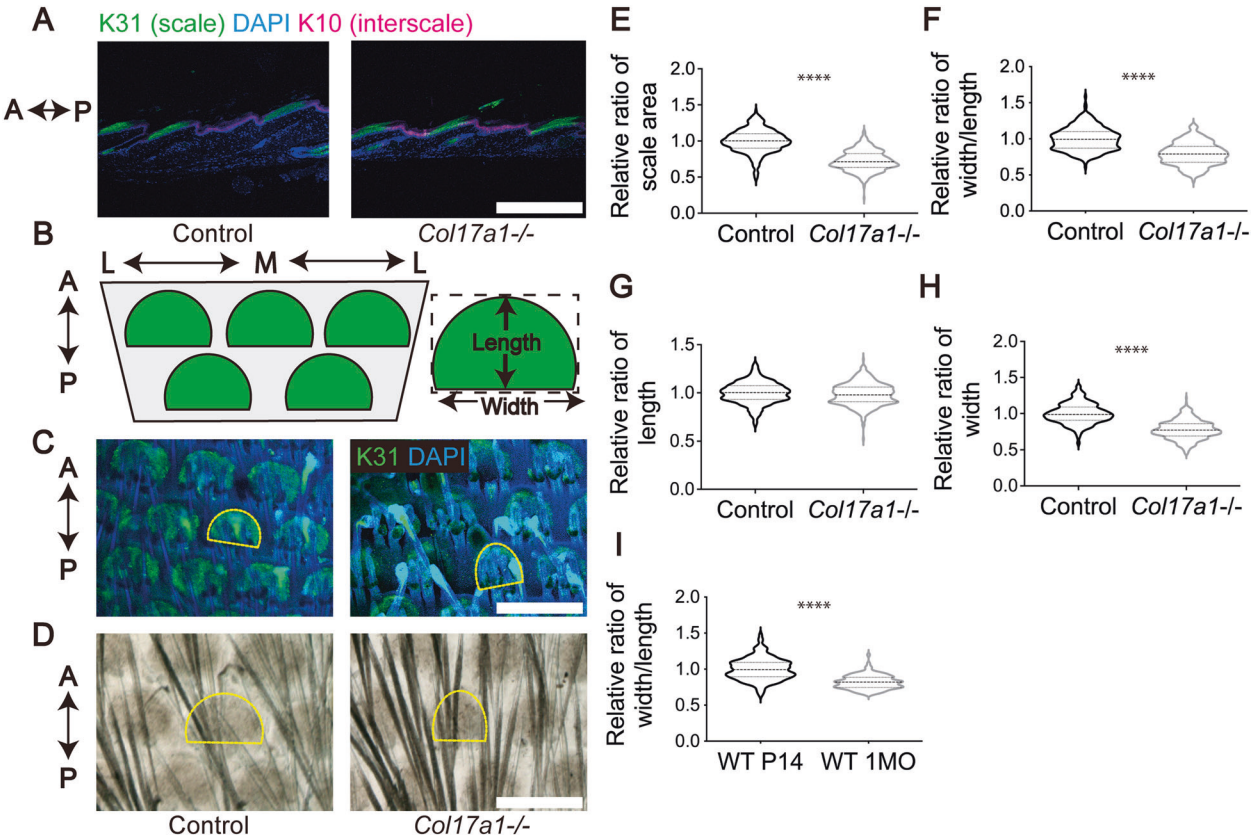

Fig. 1 Slender tail scales of *Col17a1*−/− mice. A Images showing K31 and K10 staining of *Col17a1*−/− and control tail skin samples at 1MO ($n = 4$). Scale bar: 500 μm. **B** Schematic of distribution of scales in mouse tail epidermis. **C** K31 whole-mount staining images of *Col17a1*−/− and littermate control tail epidermis at 1MO ($n = 3$). Scale bar: 500 μm. **D** Phase-contrast images of *Col17a1*−/− and littermate control tail epidermis at 1MO ($n = 4$). Scale bar: 500 μm. Quantification of the size and shape of tail scales. Scale area (**E**), width/length (**F**), length (**G**), and width (**H**) of *Col17a1*−/− and littermate control tail scales at 1MO are shown ($n = 298$ scales from three control and 413 scales from three *Col17a1*−/− mice). **I** Width/length ratio of tail scales in P14 and 1MO WT mice ($n = 148$ scales from three P14 WT mice and 123 scales from three 1MO WT mice). ****$p < 0.0001$, Welch's *t* test.

on the AP axis was comparable between *Col17a1*−/− and control scales, the cell number on the LM axis was smaller in *Col17a1*−/− scales than in control scales (Supplementary Fig. 2C), implying the altered alignment of the basal cells in *Col17a1*−/− scales. As the C57BL/6 (WT) scale shape was wider at P14 (postnatal day 14) than at 1MO (Fig. 1I), the slender scale shape in *Col17a1*−/− mice was not due to the delayed development of the mice. *Col17a1*−/− tails were generally smaller but not more slender than those of controls (Supplementary Table 1), excluding the involvement of organismal proportions in *Col17a1*−/− slender scales. Transgenic rescue by the expression of hCOL17 under the keratin 14 (K14) promoter in *Col17a1*−/− mice[19] reversed the slender scale phenotype (Fig. 2A–C). These data indicate that COL17 helps to define the scale proportion.

aPKC deregulation does not phenocopy *Col17a1*−/− scale shape

Atypical protein kinase C (aPKC) is a key regulator of epithelial polarity[28], and the epidermis expresses two aPKC isoforms (aPKCλ and aPKCζ)[29]. The ablation of aPKCλ in the epidermis (K5-Cre; $aPKC\lambda^{\Delta E5/\Delta E5}$, aPKCλ eKO) and *Col17a1*−/− mice share premature aging phenotypes such as gray hair and hair loss[15,19,21,28]. This phenotypic similarity has been proposed to be a consequence of the interaction between COL17 and the aPKC complex[30]. We asked if the destabilized aPKC accounts for the slender scale shape

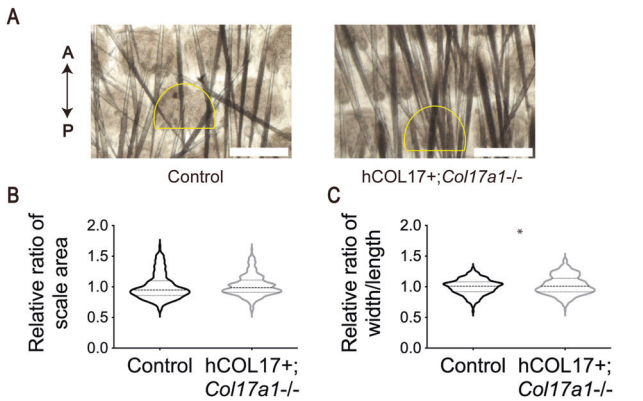

Fig. 2 Restoration of the scale shape in *Col17a1*−/− tail epidermis by human COL17 overexpression. A Whole-mount phase-contrast imaging of hCOL17+;*Col17a1*−/− and littermate control (hCOL17−; *Col17a1*+/+ or hCOL17−;*Col17a1*+/−) tail epidermis at 1MO ($n = 3$). Scale bar: 500 μm. Quantification of the size and shape of tail scales. Scale area (**B**) and width/length (**C**) of hCOL17+; *Col17a1*−/− and littermate control tail scales at 1MO are shown ($n = 266$ scales from three control and 359 scales from three hCOL17+; *Col17a1*−/− mice). The raw data used for **C** are shown in Supplementary Table 2. *$0.01 < p < 0.05$, Welch's *t*-test.

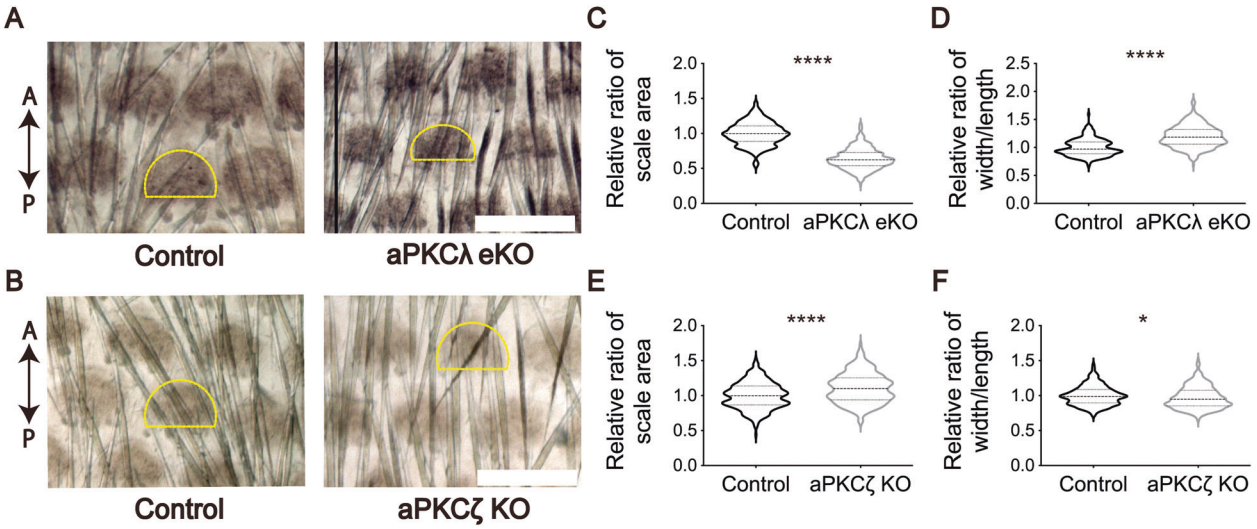

Fig. 3 Small, but not slender, tail scales of aPKCλ eKO mice. A Whole-mount phase-contrast imaging of aPKCλ eKO and littermate control tail epidermis ($n = 3$). Scale bar: 500 μm. **B** Whole-mount phase-contrast imaging of aPKCζ KO and littermate control tail epidermis ($n = 3$). Scale bar: 500 μm. Quantification of the size and shape of tail scales. Scale area and width/length of aPKCλ eKO (**C**, **D**) and aPKCζ KO (**E**, **F**) tail scales at 1MO are shown ($n = 226$ scales from three control mice and 357 scales from three aPKCλ eKO mice, $n = 300$ scales from three control mice and 317 scales from three aPKCζ KO mice). The raw data used for **F** are shown in Supplementary Table 3. ****$p < 0.0001$, *$0.01 < p < 0.05$, Welch's *t*-test.

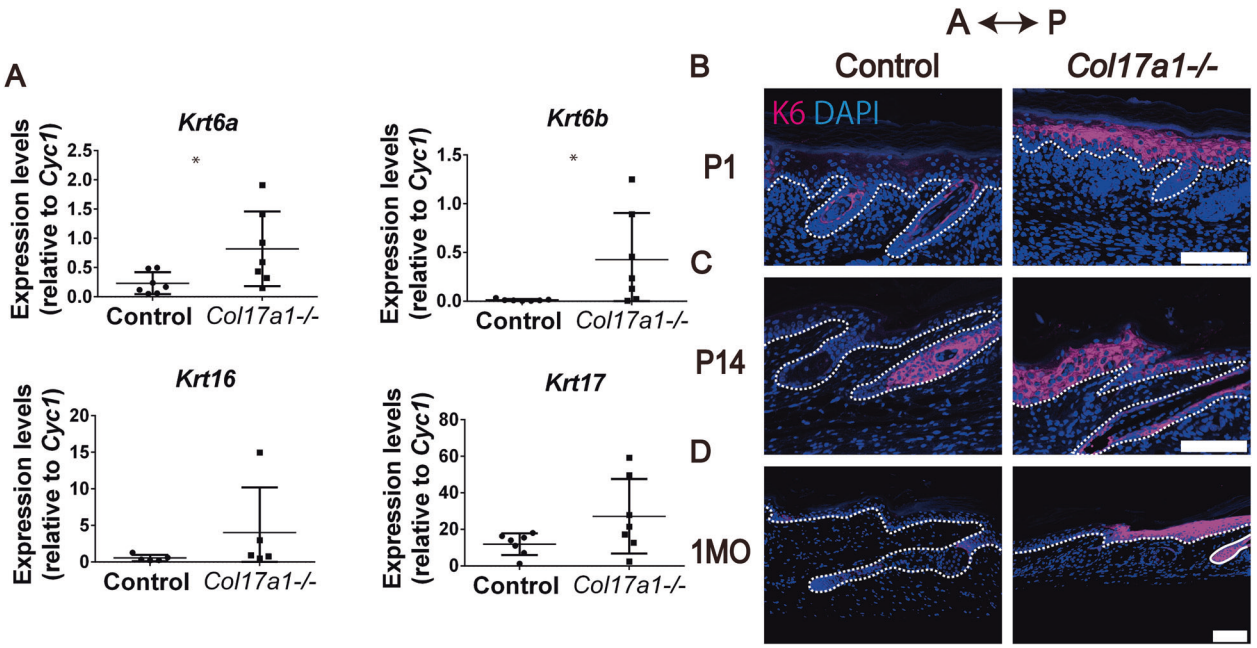

Fig. 4 Expression of wound-induced keratins in *Col17a1*−/− tail epidermis. A Gene expression of *Krt6a*, *Krt6b*, *Krt16*, and *Krt17* in the tail epidermis of *Col17a1*−/− and littermate control at 1MO ($n = 7$). *$0.01 < p < 0.05$, Student's *t*-test. K6 staining of *Col17a1*−/− and littermate control at P1 (**B**, $n = 3$), P14 (**C**, $n = 3$), and 1MO (**D**, $n = 3$). Scale bar: 100 μm.

of *Col17a1*−/− mice (Fig. 3A–F). Whole-mount imaging showed that the scale size was smaller in aPKCλ eKO than in littermate controls, but its scale proportion (width/length ratio) was wider than that of controls (Fig. 3A, C, D), which is in contrast to the slender scales of *Col17a1*−/− mice (Fig. 2). aPKCζ knockout (aPKCζ KO, *Prkcz*−/−) mice, which have no apparent skin phenotype[20], showed slightly larger scales, while the width/length ratio did not exhibit significant change (Fig. 3B, E, F). These results indicate that the aberrant cell polarity in *Col17a1*−/− epidermis[17,30] is not involved in altering the scale shape.

Expression of wound-induced keratins is pronounced in *Col17a1*−/− tail epidermis

One of the factors that may affect scale shape is the cytoskeleton of epidermal keratinocytes. Keratin 6, 16, and 17 (K6/K16/K17) are the well-known keratins expressed upon physical injury. We reasoned that these wound-induced keratins might be enriched in *Col17a1*−/− epidermis at steady state because COL17 deficiency leads to epidermolysis bullosa in humans[31] and shows skin fragility in mice[19]. Quantitative PCR revealed that the gene expression of these wound-induced keratins was higher in *Col17a1*−/− tail epidermis (Fig. 4A).

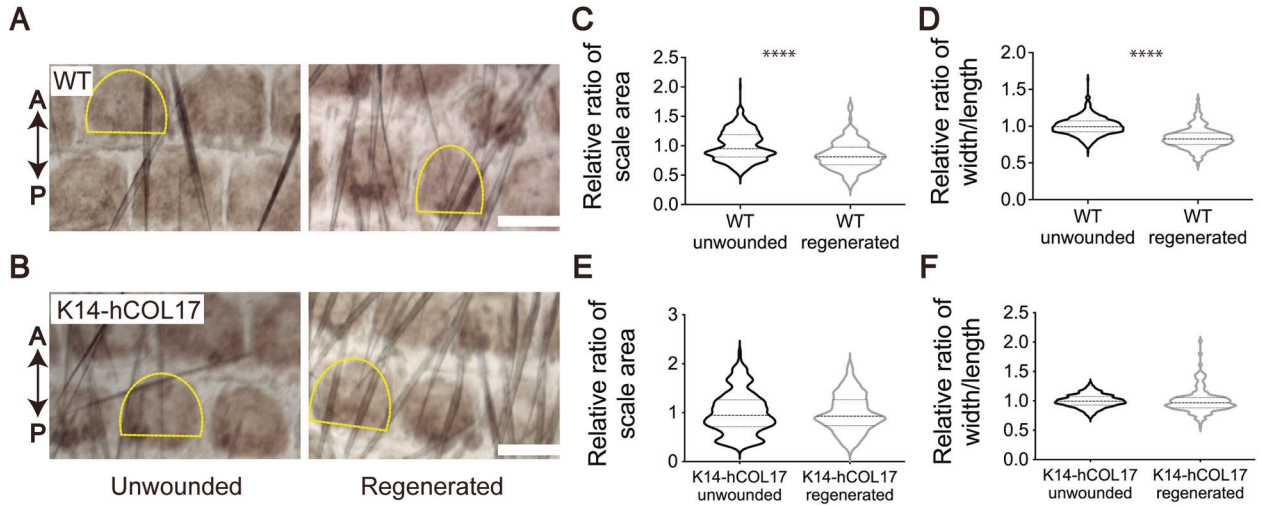

Fig. 5 Slender tail scales after skin regeneration and COL17 transgenic rescue. Whole-mount phase-contrast imaging of WT (**A**) and K14-hCOL17 (**B**) tail epidermis 4–6 weeks after wounding ($n = 4$ (WT) and 6 (K14-hCOL17), respectively). Scale bar: 500 μm. Quantification of the size and shape of tail scales. Scale area and width/length of WT (**C**, **D**) and K14-hCOL17 (**E**, **F**) tail scales after skin regeneration are shown ($n =$ 542 scales from unwounded areas and 467 scales from regenerated areas from four WT mice, $n = 424$ scales from unwounded areas and 440 scales from regenerated areas from six K14-hCOL17 mice). ****$p < 0.0001$, Welch's *t*-test.

In addition to gene expression, immunofluorescence analyses showed ectopic K6 expression in *Col17a1*−/− tail epidermis at 1MO. K6 expression in *Col17a1*−/− tail epidermis was also observed during the developmental stages (P1 and P14; Fig. 4B–D). These data indicate that keratin profiles are skewed towards the wound-induced subsets in *Col17a1*−/− epidermis. In contrast, human or murine cultured keratinocytes knocked down for *COL17A1 or Col17a1* did not result in the expression of wound-induced keratins at the mRNA or protein level (Supplementary Figs. 3 and 4), suggesting that this phenotype is dependent on the in vivo setting. Rather, *KRT16* and *Krt6b* expression was reduced in human and murine knockdown experiments, respectively, for unknown reasons.

Scale shape becomes slender after skin regeneration, and COL17 overexpression rescues the phenotype

The expression of wound-induced keratins in *Col17a1*−/− epidermis led us to ask whether wounding itself alters the tail scale shape upon skin regeneration (Fig. 5A–F). The regenerated tail epidermis (4 to 6 weeks after wounding) exhibited a more slender scale shape than the non-lesional areas (Fig. 5A, C, D), recapitulating the *Col17a1*−/− scale (Fig. 2). The slender scale phenotype in the regenerated epidermis was not reversed 3 months after wounding (Supplementary Fig. 5B–D). To see that additive COL17 prevents the alteration of the scale shape in the regenerated epidermis, we utilized K14-hCOL17 transgenic mice, which overexpress hCOL17 under the K14 promoter. The scale shape of the regenerated K14-hCOL17 skin was not as slender as that of the regenerated WT skin (Fig. 5B, E, F). These results suggest that COL17 prevents wound-induced scale deformation.

COL17 influences human skin microtopography

We finally asked whether the presence or absence of COL17 also affects epidermal patterning in humans. Although scale/interscale epidermal patterns in mouse tails are not conserved, skin surface patterns consisting of grooves and ridges are visible in humans. We took advantage of the revertant mosaicism in epidermolysis bullosa (EB), in which the mutated genes are corrected spontaneously[32,33]. We compared COL17-negative (diseased) and COL17-positive (revertant) skin from a junctional EB (JEB) patient with *COL17A1* mutations[23] (Fig. 6A–C, Supplementary Fig. 6). The diseased skin surface appeared coarse, while the revertant skin was smooth (Fig. 6B). We calculated the auto-correlation functions of these skin images to quantify the skin microtopography and found that the diseased skin shows a distinct pattern from the revertant skin (Fig. 6D). These findings demonstrate that COL17 is a deterministic factor of epidermal patterning in mice and humans.

DISCUSSION

COL17 is a hemidesmosomal protein that anchors basal keratinocytes to the dermis. COL17 stabilizes hemidesmosomes by binding to various basement membrane zone proteins including BP230[34,35], α6 integrin[36], β4 integrin[35,37–39], plectin[35,40], laminin-332[25,41], and type IV collagen[42,43]. As a consequence, COL17 deficiency results in epidermolysis bullosa[19,31]. Recently, COL17 has also been highlighted as an SC niche protein of HFs and epidermis, and its deficiency destabilizes epithelial SC maintenance[7,15–17]. Our study provides new insights into COL17 biology. *Col17a1*−/− mice have slender tail scales and are characterized by the expression of wound-induced keratins in the epidermis. In line with this, the regenerated epidermis after wounding shows slender tail scales. Human COL17 overexpression reverses the alteration of scale shapes upon wounding (Fig. 7).

Epidermal cell polarity regulates symmetrical and asymmetrical cell division of basal keratinocytes[44–46] and is regulated by the aPKC complex[47–49]. Increased asymmetrical cell division in aPKCλ eKO epidermis[28] and possible SC depletion explain the smaller scales in aPKCλ eKO mice (Fig. 3). Although COL17 interacts with the aPKC complex[30] and helps maintain epidermal cell polarity[17,30], *Col17a1*−/− did not exhibit proportionally small scales as seen in aPKCλ eKO mice. This phenotypical difference indicates that the slender scale phenotype in *Col17a1*−/− mice is independent of aberrant cell polarity.

A limitation of our study is that it does not explain which contributes more to the altered epidermal patterns in *Col17a1*−/− mice: epidermal SC instability or weakened epidermal-dermal adhesion. As the HF abnormality of *Col17a1*−/− mice becomes apparent at 3 months old[15], it is not very likely that HFs are involved in the phenotypes of epidermal patterns at 1 month old in our study. Furthermore, the hard palate in the oral mucosa, where HFs are absent, shows an epithelial pattern of fast- and slow-cycling SCs[50], recapitulating the epidermal pattern of the tail

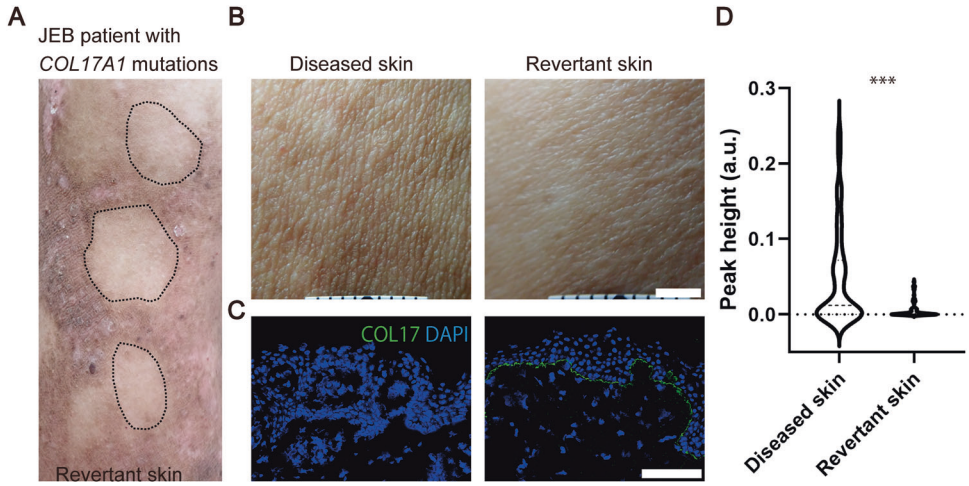

Fig. 6 Distinct epidermal patterns of COL17-positive and negative human skin. A The upper arm of a junctional epidermolysis bullosa patient who is compound heterozygous for c.1179del (p.Ala394Leufs*9) and c.4159C>T (p.Gln1387*) in *COL17A1* (NM_000494.4). The revertant skin areas are circled by dotted lines. **B** Representative images of the diseased and revertant skin. Scale bar: 3 mm. These images are exemplified in Supplementary Fig. 6. **C** COL17 labeling of the diseased and revertant skin. Scale bar: 100 μm. **D** Quantification of skin microtopography ($n = 75$ spots (radius: 3 mm) from three skin areas, respectively). The degree of regularity on the epidermal pattern was quantified by the peak height of the autocorrelation function (Supplementary Fig. 6). ***$0.0001 < p < 0.001$, Mann–Whitney test.

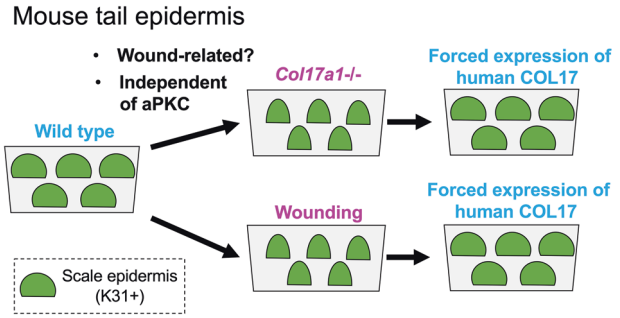

Fig. 7 COL17-related epidermal patterning. A graphical abstract of the study. COL17 deficiency or wounding leads to slender scale epidermis, which is reversed by overexpression of human COL17 in the epidermis.

skin. Thus, HFs might not be essential for epithelial pattern formation.

Among various skin patterns, fingerprints, also called dermatoglyphics, are the most well characterized in humans. Fingerprints show an alternate pattern of epidermal ridges and grooves. Loss of fingerprints has been described in EB patients, including Kindler syndrome[51,52] and JEB with *COL17A1* p.Arg1303Gln mutation[24–26]. Our study has also demonstrated that the presence of COL17 alters human skin microtopography (Fig. 6). These facts corroborate the role of COL17 in epidermal patterning and highlight COL17 as a therapeutic target for wound-induced skin deformations.

Human skin microtopography is not identical to mouse tail scale patterns because humans lost their tails after evolutionarily branching off from other primates. It has not been determined whether human skin ridges or grooves correspond to the fast- or slow-cycling areas that characterize mouse tails. However, the data that COL17 absence disturbs proper skin patterning in both humans and mice point to the involvement of COL17 in regulating skin surface texture across species.

Wound repair in mouse back skin requires wound contraction[53]; however, the contribution of wound contraction has been regarded as minimal in the tail skin[54]. Recent studies suggest that two-thirds of tail wound healing is due to epithelial regeneration, while wound contraction explains the remainder[55]. We believe that wound contraction does not play a major role in the slender scale phenotype in the regenerated tail skin (Fig. 5) for the following reasons: (1) the scale shape in the regenerated skin would become proportionally small rather than slender if the wound contraction affected this phenotype, and (2) the slender scale phenotype in the regenerated skin is rescued by K14-driven human COL17 overexpression, which might not influence wound contraction because the transgene expression is confined to the epidermis. The slender scales in *Col17a1*−/− mice most likely represent wound-related skin changes that involve the expression of wound-induced keratins in *Col17a1*−/− epidermis (Fig. 4). However, the mechanisms by which wound-related skin changes affect epidermal patterning need further investigation.

In conclusion, our study highlights the unrecognized role of COL17 in epidermal patterning. We propose that COL17 modulation can be utilized to prevent epidermal deformation upon wounding.

DATA AVAILABILITY

The datasets used and/or analyzed during the current study are available from the corresponding author on reasonable request.

REFERENCES

1. Natsuga, K. Epidermal barriers. *Cold Spring Harb. Perspect. Med.* **4**, a018218 (2014).
2. Moreci, R. S. & Lechler, T. Epidermal structure and differentiation. *Curr. Biol.* **30**, R144–R149 (2020).
3. Natsuga, K., Watanabe, M., Nishie, W. & Shimizu, H. Life before and beyond blistering: the role of collagen XVII in epidermal physiology. *Exp. Dermatol.* **28**, 1135–1141 (2019).
4. Watt, F. M. & Fujiwara, H. Cell-extracellular matrix interactions in normal and diseased skin. *Cold Spring Harb. Perspect. Biol.* **3**, a005124 (2011).
5. Brakebusch, C. et al. Skin and hair follicle integrity is crucially dependent on β1 integrin expression on keratinocytes. *EMBO J.* **19**, 3990–4003 (2000).
6. Niculescu, C. et al. Conditional ablation of integrin alpha-6 in mouse epidermis leads to skin fragility and inflammation. *Eur. J. Cell Biol.* **90**, 270–277 (2011).
7. Watanabe, M. et al. Type XVII collagen coordinates proliferation in the interfollicular epidermis. *Elife* **6**, e26635 (2017).
8. Dekoninck, S. et al. Defining the design principles of skin epidermis postnatal growth. *Cell* **181**, 604–620 (2020).
9. Gomez, C. et al. The interfollicular epidermis of adult mouse tail comprises two distinct cell lineages that are differentially regulated by Wnt, Edaradd, and Lrig1. *Stem Cell Rep.* **1**, 19–27 (2013).

10. Sada, A. et al. Defining the cellular lineage hierarchy in the interfollicular epidermis of adult skin. *Nat. Cell Biol.* **18**, 619–631 (2016).
11. Jones, P. H., Harper, S. & Watt, F. M. Stem cell patterning and fate in human epidermis. *Cell* **80**, 83–93 (1995).
12. Kobayashi, Y. et al. Interplay between epidermal stem cell dynamics and dermal deformation. *Npj Comput. Mater.* **4**, 1–9 (2018).
13. Wang, S. et al. Single cell transcriptomics of human epidermis identifies basal stem cell transition states. *Nat. Commun.* **11**, 1–14 (2020).
14. López-Rovira, T., Silva-Vargas, V. & Watt, F. M. Different consequences of β1 integrin deletion in neonatal and adult mouse epidermis reveal a context-dependent role of integrins in regulating proliferation, differentiation, and intercellular communication. *J. Investig. Dermatol.* **125**, 1215–1227 (2005).
15. Tanimura, S. et al. Hair follicle stem cells provide a functional niche for melanocyte stem cells. *Cell Stem Cell* **8**, 177–187 (2011).
16. Matsumura, H. et al. Hair follicle aging is driven by transepidermal elimination of stem cells via COL17A1 proteolysis. *Science* **351**, aad4395 (2016).
17. Liu, N. et al. Stem cell competition orchestrates skin homeostasis and ageing. *Nature* **568**, 344–350 (2019).
18. Hirate, Y. et al. Polarity-dependent distribution of angiomotin localizes Hippo signaling in preimplantation embryos. *Curr. Biol.* **23**, 1181–1194 (2013).
19. Nishie, W. et al. Humanization of autoantigen. *Nat. Med.* **13**, 378–383 (2007).
20. Noguchi, N. et al. Atypical protein kinase C isoforms differentially regulate directional keratinocyte migration during wound healing. *J. Dermatol. Sci.* **93**, 101–108 (2019).
21. Osada, S.-I. et al. Atypical protein kinase C isoform, aPKCλ, is essential for maintaining hair follicle stem cell quiescence. *J. Investig. Dermatol.* **135**, 2584–2592 (2015).
22. Yuspa, S. H., Hawley-Nelson, P., Koehler, B. & Stanley, J. R. A survey of transformation markers in differentiating epidermal cell lines in culture. *Cancer Res.* **40**, 4694–4703 (1980).
23. Nakamura, H. et al. Analysis of the COL17A1 in non-Herlitz junctional epidermolysis bullosa and amelogenesis imperfecta. *Int. J. Mol. Med.* **18**, 333–337 (2006).
24. Yuen, W., Pas, H., Sinke, R. & Jonkman, M. Junctional epidermolysis bullosa of late onset explained by mutations in COL17A1. *Br. J. Dermatol.* **164**, 1280–1284 (2011).
25. Nishimura, M. et al. Extracellular cleavage of collagen XVII is essential for correct cutaneous basement membrane formation. *Hum. Mol. Genet.* **25**, 328–339 (2016).
26. Stouthamer, A., Nieboer, C., Van der Waal, R. & Jonkman, M. Normal expression of the 19-DEJ-1 epitope in two siblings with late-onset junctional epidermolysis bullosa. *Br. J. Dermatol.* **144**, 1054–1057 (2001).
27. Okada, M., Sumino, Y., Ito, H. & Kitahata, H. Spontaneous deformation and fission of oil droplets on an aqueous surfactant solution. *Phys. Rev. E* **102**, 042603 (2020).
28. Niessen, M. T. et al. aPKCλ controls epidermal homeostasis and stem cell fate through regulation of division orientation. *J. Cell Biol.* **202**, 887–900 (2013).
29. Helfrich, I. et al. Role of aPKC isoforms and their binding partners Par3 and Par6 in epidermal barrier formation. *J. Investig. Dermatol.* **127**, 782–791 (2007).
30. Watanabe, M. et al. Type XVII collagen interacts with the aPKC-PAR complex and maintains epidermal cell polarity. *Exp. Dermatol.* **30**, 62–67 (2021).
31. McGrath, J. A. et al. Mutations in the 180–kD bullous pemphigoid antigen (BPAG2), a hemidesmosomal transmembrane collagen (COL17A1), in generalized atrophic benign epidermolysis bullosa. *Nat. Genet.* **11**, 83–86 (1995).
32. Jonkman, M. F. & Pasmooij, A. M. Revertant mosaicism—patchwork in the skin. *N. Engl. J. Med.* **360**, 1680–1682 (2009).
33. Nomura, T. Recombination-induced revertant mosaicism in ichthyosis with confetti and loricrin keratoderma. *J. Dermatol. Sci.* **97**, 94–100 (2020).
34. Hopkinson, S. B. & Jones, J. C. The N terminus of the transmembrane protein BP180 interacts with the N-terminal domain of BP230, thereby mediating keratin cytoskeleton anchorage to the cell surface at the site of the hemidesmosome. *Mol. Biol. Cell.* **11**, 277–286 (2000).
35. Koster, J., Geerts, D., Favre, B., Borradori, L. & Sonnenberg, A. Analysis of the interactions between BP180, BP230, plectin and the integrin α6β4 important for hemidesmosome assembly. *J. Cell Sci.* **116**, 387–399 (2003).
36. Hopkinson, S. B., Baker, S. E. & Jones, J. Molecular genetic studies of a human epidermal autoantigen (the 180-kD bullous pemphigoid antigen/BP180): identification of functionally important sequences within the BP180 molecule and evidence for an interaction between BP180 and alpha 6 integrin. *J. Cell Biol.* **130**, 117–125 (1995).
37. Aho, S. & Uitto, J. Direct interaction between the intracellular domains of bullous pemphigoid antigen 2 (BP180) and β4 integrin, hemidesmosomal components of basal keratinocytes. *Biochem. Biophys. Res. Commun.* **243**, 694–699 (1998).
38. Schaapveld, R. Q. et al. Hemidesmosome formation is initiated by the β4 integrin subunit, requires complex formation of β4 and HD1/plectin, and involves a direct interaction between β4 and the bullous pemphigoid antigen 180. *J. Cell. Biol.* **142**, 271–284 (1998).
39. Hamill, K. J., Hopkinson, S. B., Jonkman, M. F. & Jones, J. C. Type XVII collagen regulates lamellipod stability, cell motility, and signaling to Rac1 by targeting bullous pemphigoid antigen 1e to α6β4 integrin. *J. Biol. Chem.* **286**, 26768–26780 (2011).
40. Natsuga, K. et al. Loss of interaction between plectin and type XVII collagen results in epidermolysis bullosa simplex. *Hum. Mutat.* **38**, 1666–1670 (2017).
41. Tasanen, K., Tunggal, L., Chometon, G., Bruckner-Tuderman, L. & Aumailley, M. Keratinocytes from patients lacking collagen XVII display a migratory phenotype. *Am. J. Pathol.* **164**, 2027–2038 (2004).
42. Nishie, W., Kiritsi, D., Nyström, A., Hofmann, S. C. & Bruckner-Tuderman, L. Dynamic interactions of epidermal collagen XVII with the extracellular matrix: laminin 332 as a major binding partner. *Am. J. Pathol.* **179**, 829–837 (2011).
43. Kamaguchi, M. & Iwata, H. The diagnosis and blistering mechanisms of mucous membrane pemphigoid. *Front. Immunol.* **10**, 34 (2019).
44. Morrow, A., Underwood, J., Seldin, L., Hinnant, T. & Lechler, T. Regulated spindle orientation buffers tissue growth in the epidermis. *Elife* **8**, e48482 (2019).
45. Muroyama, A. & Lechler, T. Polarity and stratification of the epidermis. *Semin. Cell Dev. Biol.* **23**, 890–896 (2012).
46. Poulson, N. D. & Lechler, T. Asymmetric cell divisions in the epidermis. *Int. Rev. Cell Mol. Biol.* **295**, 199–232 (2012).
47. Niessen, M. T., Iden, S. & Niessen, C. M. The in vivo function of mammalian cell and tissue polarity regulators–how to shape and maintain the epidermal barrier. *J. Cell Sci.* **125**, 3501–3510 (2012).
48. Tellkamp, F., Vorhagen, S. & Niessen, C. M. Epidermal polarity genes in health and disease. *Cold Spring Harb. Perspect. Med.* **4**, a015255 (2014).
49. Vorhagen, S. & Niessen, C. M. Mammalian aPKC/Par polarity complex mediated regulation of epithelial division orientation and cell fate. *Exp. Cell Res.* **328**, 296–302 (2014).
50. Byrd, K. M. et al. Heterogeneity within Stratified Epithelial Stem Cell Populations Maintains the Oral Mucosa in Response to Physiological Stress. *Cell Stem Cell* **25**, 814–829 e816 (2019).
51. Has, C. et al. Mild clinical phenotype of Kindler syndrome associated with late diagnosis and skin cancer. *Dermatology* **221**, 309–312 (2010).
52. de Almeida, H. L. Jr, Isaacsson, H., Guarenti, I. M., e Silva, R. M. & de Castro, L. A. S. Images in dermatology. *An. Bras. Dermatol.* **90**, 581–584 (2015).
53. Grada, A., Mervis, J. & Falanga, V. Research techniques made simple: animal models of wound healing. *J. Investig. Dermatol.* **138**, 2095–2105. e2091 (2018).
54. Falanga, V. et al. Full-thickness wounding of the mouse tail as a model for delayed wound healing: accelerated wound closure in Smad3 knock-out mice. *Wound Repair Regen.* **12**, 320–326 (2004).
55. Aragona, M. et al. Defining stem cell dynamics and migration during wound healing in mouse skin epidermis. *Nat. Commun.* **8**, 1–14 (2017).

ACKNOWLEDGEMENTS

We thank Ms. Megumi Takehara for their technical assistance. We also thank Professor Kim B. Yancey for providing K14-hCOL17 transgenic mice.

AUTHOR CONTRIBUTIONS

Y.W. performed the experiments, analyzed the data, interpreted the results, and wrote the manuscript. H.Kitahata analyzed the data, interpreted the results, and wrote the manuscript. H.Kosumi, M.W., Y.F., S.T., S.I.O., T.H., and W.N. performed the experiments and analyzed the data. M.N. and H.S. interpreted the results and supervised the study. K.N. designed the experiments, analyzed the data, interpreted the results, wrote the manuscript and supervised the study.

FUNDING

This work was funded by AMED to K.N. (20ek0109380h0003), the Lydia O'Leary Memorial Pias Dermatological Foundation to W.N., JST CREST (JPMJCR15D2) to M.N., and Five-star Alliance in NJRC Master. & Dev to H.Kitahata/M.N.

COMPETING INTERESTS

The authors declare no competing interests.

ETHICS APPROVAL AND CONSENT TO PARTICIPATE

The institutional review board of the Hokkaido University Graduate School of Medicine approved all human studies described above (ID: 13-043). The study was conducted according to the principles of the Declaration of Helsinki. The participant provided written informed consent.

ADDITIONAL INFORMATION

Supplementary information The online version contains supplementary material available at https://doi.org/10.1038/s41374-022-00738-2.

Correspondence and requests for materials should be addressed to Ken Natsuga.